Water Supply

IWA PUBLISHING



Water Supply Vol 22 No 3, 2750 doi: 10.2166/ws.2021.439

# The performance of calcined serpentine to simultaneously remove fluoride, iron and manganese

Xilin Li, Qi Wang, Ling Liu* and Siyuan Liu

College of Civil Engineering, Liaoning Technical University, No. 88, Yulong Road, Xihe District, Fuxin, Liaoning Province 123000, China
*Corresponding author. E-mail: liuling@lntu.edu.cn

XL, 0000-0003-0870-4996; QW, 0000-0002-5882-2715; LL, 0000-0002-8154-0556; SL, 0000-0002-3770-2220

## ABSTRACT

To solve the problem of high fluoride, iron and manganese concentrations in groundwater, serpentine (Srp) was modified by metal salt impregnation, acid–base activation and calcination, and the effects of these three modifications on the removal performance of Srp were compared. Specifically, the effects of the calcined serpentine (Csrp) dose, reaction time, pH, and temperature on the removal performance of $F^-$, $Fe^{2+}$ and $Mn^{2+}$ on Csrp were analysed. An isothermal adsorption model and adsorption kinetic equation were established and confirmed through SEM, EDS, XRD and FTIR spectroscopy to analyse the mechanism of removing $F^-$, $Fe^{2+}$ and $Mn^{2+}$ by Csrp. The results show that when 3 g/L Csrp was used to treat water samples with 5 mg/L $F^-$, 20 mg/L $Fe^{2+}$, and 5 mg/L $Mn^{2+}$ (pH of 6, reaction temperature of 35 °C, and time of 150 min), the removal rates of $F^-$, $Fe^{2+}$, and $Mn^{2+}$ were 94.3%, 99.0%, 98.9%, respectively. The adsorption of $F^-$, $Fe^{2+}$ and $Mn^{2+}$ on Csrp follows the quasi-second-order kinetic equation and Langmuir isotherm adsorption model. After five cycles of regeneration of Csrp, Csrp can still maintain good properties of fluoride, iron and manganese removal.

**Key words:** calcined modification, fluoride, iron, manganese, removal mechanism, serpentine

## HIGHLIGHTS

- Microscopic characterization of calcined serpentine was carried out.
- Calcined serpentine can achieve the synchronous removal of high fluoride, iron and manganese concentrations in groundwater.
- The adsorption isothermal model and adsorption kinetic equation of calcined serpentine were established.
- The mechanism for the simultaneous removal of fluoride, iron and manganese by calcined serpentine was analysed.

## GRAPHICAL ABSTRACT

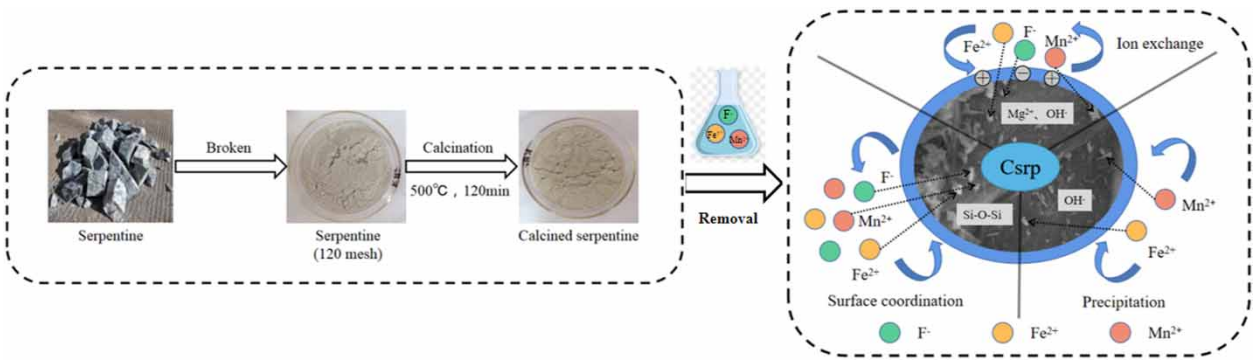


## INTRODUCTION

Excessive fluoride, iron and manganese in groundwater have an impact on the health of residents, and there are problems related to high levels of fluoride, iron and manganese in groundwater both at home and abroad (Li *et al.* 2021a). Fluoride

is widely present in minerals, natural water systems and geological deposits and enters the food chain through human consumption or vegetation (Jin *et al.* 2016). The excessive intake of fluoride affects human health and causes fluorosis (Cai *et al.* 2015). Iron and manganese ions exist in nature in the form of dissolved single ions ($Fe^{2+}$, $Mn^{2+}$) or in the form of undissolved $Fe(OH)_3$ and $MnO_2$ (Barloková & Ilavský 2010). $Fe^{2+}$ and $Mn^{2+}$ form hydroxides after oxidation, which affects the colour, taste and turbidity of water (Homoncik *et al.* 2010). These insoluble hydroxides can produce toxic derivatives in the body and cause many physical diseases. The World Health Organization stipulates that the maximum limit of fluoride is 1.5 mg/L (Zawar *et al.* 2020). The EU Directive 2020/2184 sets the following limits for aesthetic reasons: Fe $<$ 0.2 mg/L and Mn $<$ 0.05 mg/L. Therefore, the removal of fluoride, iron, and manganese from groundwater is an urgent need to solve the problem of using groundwater that contains fluoride, iron, and manganese as drinking water.

There are many studies on the separate removal of fluoride, iron and manganese (Kwakye-Awuah *et al.* 2019; Yadav *et al.* 2019; Aziz *et al.* 2020). However, there are few studies on their simultaneous removal, and thus, it is essential to explore how to simultaneously remove fluoride, iron and manganese in groundwater (Zhang *et al.* 2009). At present, the methods for treating fluoride-containing groundwater mainly include ion exchange, electrolysis, reverse osmosis, nanofiltration and adsorption (Abri *et al.* 2019). The main approaches to treat groundwater containing iron and manganese include filtration, contact oxidation, microbial treatment, ion exchange, ultra/microfiltration membranes, and adsorption (Chaturvedi & Dave 2012; Patil *et al.* 2016). Among the above methods, the adsorption method is the first choice to remediate groundwater pollution due to its low cost, high adsorption capacity, and low energy consumption (Meski *et al.* 2019). Optimizing adsorbents for the simultaneous removal of fluorine, iron and manganese is the key to research and application. Natural minerals are inexpensive and have good chemical stability; thus, they are often used to adsorb fluoride or heavy metal ions from water. Serpentine, as a magnesium-rich silicate mineral, exists abundant reserves in China and is widely distributed throughout areas such as the Liaoning Province and Shanxi Province. Serpentine itself contains a large number of active groups, such as hydroxyl groups and unsaturated Si-O-Si, O-Si-O, magnesium and hydrogen bonds, which can be combined with metal ions to undergo ion exchange and surface coordination reactions (Cattaneo *et al.* 2003; Shaban *et al.* 2018). Thus, the adsorption performance of modified serpentine can be significantly improved. Mobarak *et al.* (2019) used chemically modified serpentine to remove $Cr^{6+}$ and $F^-$ at rates of 87.31% and 94.72%, respectively. Huang *et al.* (2017) used mechanically activated serpentine to remove $Cu^{2+}$ from water, and this modified serpentine exhibited a significant increase in adsorption capacity compared with natural serpentine.

Based on the above results, this article first studies the modification of Srp and selects the best modification method. The effects of the Csrp dose, reaction time, pH, and temperature on the removal effect of $F^-$, $Fe^{2+}$, $Mn^{2+}$ were also explored. An isothermal adsorption model and adsorption kinetic equation were established to investigate the adsorption behaviour of Csrp for $F^-$, $Fe^{2+}$ and $Mn^{2+}$. The adsorption performance of Csrp for $F^-$, $Fe^{2+}$ and $Mn^{2+}$ in water was compared with other adsorbents. The removal mechanism of Csrp for $F^-$, $Fe^{2+}$ and $Mn^{2+}$ was revealed by SEM, EDS, XRD, and FTIR spectroscopy, which provides a reference for further studies on the simultaneous removal of $F^-$, $Fe^{2+}$ and $Mn^{2+}$ from groundwater.

## MATERIALS AND METHODS

### Experimental materials

Srp was obtained from the boron mining area in Yingkou City, Liaoning Province, China, and ground to 120 mesh. The test reagents included $Al_2(SO_4)_3{\cdot}18H_2O$, $CaCl_2$, NaOH, HCl, $MnSO_4{\cdot}3H_2O$, $FeSO_4{\cdot}7H_2O$, NaF, $NaCO_3$, $HNO_3$, $NH_3{\cdot}H_2O$, $C_{12}H_8N_2{\cdot}H_2O$, $CH_3COOH$, and $C_{14}H_{22}N_2O_8{\cdot}H_2O$, all of analytical grade, which were purchased from the Liaoning Quanrui Reagent Co., Ltd.

### Test instrument

An electronic balance (e = 10d) was used to weigh the test materials. The adsorption reaction was carried out in an intelligent precision shaker (BXD-YX-2000), and calcination was carried out in a box resistance furnace (SRJX-4-10). The $F^-$ concentration was determined by a fluoride ion selective electrode (PF-2-01), and the concentrations of $Fe^{2+}$ and $Mn^{2+}$ were determined by an atomic absorption spectrophotometer (Z-2000). A precision pH meter (PHS-3C) was used to measure the pH. Scanning electron microscopy (SEM, Hitachi S-3400N) was used to observe the apparent morphological changes in the sample. Energy dispersive X-ray spectroscopy (EDS, FEI Quanta TM250) was used to qualitatively and quantitatively analyse each element in the sample. X-ray diffraction (XRD, D8 ADVANCE) was used for phase analysis of Csrp before and

after the reaction. Fourier transform infrared (FTIR, AVATAR 330) spectroscopy was used to analyse changes in the functional groups before and after adsorption by the sample.

### Preparation of modified serpentine

Srp was modified by the following methods:

Impregnation of a metal salt: Two hundred millilitres of aluminium sulfate solution and calcium chloride solution with mass fractions of 1%, 2%, 3%, 4%, 5%, 6%, and 7% were prepared. Then, 10 g of 120 mesh Srp was added to each solution, which was fully stirred for 3 h, aged for 24 h, filtered to remove the Srp, washed with distilled water and dried for later use.

Acid–base activation: Two hundred millilitres of hydrochloric acid solution and sodium hydroxide solution with mass fractions of 1%, 2%, 3%, 4%, 5%, 6%, and 7% were prepared. Then, 10 g of 120 mesh Srp was added to each solution, fully stirred for 3 h, aged for 24 h, filtered to remove the Srp, washed with distilled water and dried for later use.

Calcination: Srp (50 g, 120 mesh) was calcined for 120 min in a box resistance furnace at 100, 200, 300, 400, 500, 600 and 700 °C. After calcination was completed, the serpentine was sealed and stored.

### Preparation of dealkalized Csrp

Ten grams of Csrp were placed in a 500 mL conical flask, and a certain amount of distilled water was added to dealkali the particles. The distilled water in the conical bottle was replaced at regular intervals until the particles no longer released alkalinity. The dealkalized particles were put into the oven to dry until a constant weight was reached.

### Test water sample

The groundwater in Fuxin City, Liaoning Province, China, contains high concentrations of fluoride (1.5–5.0 mg/L), iron (3.5–19.5 mg/L) and manganese (0.9–4.8 mg/L), and the pH is between 6.0 and 6.8. Due to the low oxygen content in the groundwater, iron and manganese are not easily oxidized and are often dissolved in the groundwater in the forms of $Fe^{2+}$ and $Mn^{2+}$. Thus, they were used as the research objects in this work. Considering the instability and complexity of actual groundwater, experimental water samples were configured to simulate the groundwater quality in the Fuxin area. The mass concentrations of $F^-$, $Fe^{2+}$ and $Mn^{2+}$ in the water samples were 5, 20 and 5 mg/L, respectively, and the pH was adjusted to 6.5. In addition, to prevent $Fe^{2+}$ and $Mn^{2+}$ from being oxidized during the adsorption process, a nitrogen cylinder was used to keep the shaker box filled with nitrogen. Xie *et al.* (2015) also used this method when studying the adsorption of $Fe^{2+}$ and $S^{2-}$ by fermented rice husks.

### Experimental method

#### Modified Srp to remove fluoride, iron and manganese experiment

Briefly, 150 mL of a composite water sample was added to an Erlenmeyer flask. Then, 300 mg of differently modified Srp was added to the flask, shaken, and then allowed to react for 120 min in a shaker at 180 rpm and 25 °C. Finally, the mass concentrations of $F^-$, $Fe^{2+}$, and $Mn^{2+}$ were measured.

### Experiments on the influence of Csrp removal performance

The effects of the dose, reaction time, pH and reaction temperature on the removal of $F^-$, $Fe^{2+}$ and $Mn^{2+}$ by Csrp were investigated through batch tests. The adsorption capacity and removal rate of $F^-$, $Fe^{2+}$ and $Mn^{2+}$ by Csrp can be calculated using Equations (1) and (2):

$$q_e = \frac{(c_0 - c_e)V}{m} \tag{1}$$

$$R = \frac{(c_0 - c_e)}{c_0} \times 100\% \tag{2}$$

where $q_e$ is the adsorption capacity at equilibrium, mg/g; $c_0$ is the initial concentration of solution, mg/L; $c_e$ is the concentration of solution at adsorption equilibrium, mg/L; $V$ is the volume of solution, L; and $m$ is the mass of adsorbent, g.

### Experiments on the influence of dealkalized Csrp removal performance

A total of 450 mg of dealkalized Csrp was weighed and added into 150 mL of a composite water sample containing $F^-$, $Fe^{2+}$ and $Mn^{2+}$. The reaction was carried out in a constant temperature shaker at 35 °C, and the samples were sampled and filtered at a predetermined time to determine the concentrations of $F^-$, $Fe^{2+}$ and $Mn^{2+}$ in the filtrate.

### Adsorption kinetics

Briefly, 450 mg of Csrp was weighed and added to 150 mL of a composite water sample containing $F^-$, $Fe^{2+}$ and $Mn^{2+}$. The oscillating reaction was carried out under optimal adsorption conditions (pH of 6, temperature of 35 °C). Samples were taken and filtered at predetermined times to determine the concentrations of $F^-$, $Fe^{2+}$ and $Mn^{2+}$ in the filtrate. Quasi-first-order and quasi-second-order rate equations are often used to describe and analyse the kinetic process of solid–liquid adsorption, and the fitted correlation coefficient $R^2$ is used for fitting evaluation (Ijagbemi *et al.* 2010). The equations are as follows (Equations (3) and (4)):

Quasi-first-order kinetic equation:

$$\lg(q_e - q_t) = \lg(q_e) - \left(\frac{k_1}{2.303}\right)t \tag{3}$$

Quasi-second-order kinetic equation:

$$\frac{t}{q_t} = \frac{1}{k_2 \cdot q_e^2} + \frac{t}{q_e} \tag{4}$$

where $q_t$ (mg/g) is the amount of adsorbent at time t (min) and $k_1$ and $k_2$ are the adsorption rate constants, $min^{-1}$.

### Adsorption isotherm

Briefly, 450 mg of Csrp was weighed and added to 150 mL of a composite water sample containing $F^-$, $Fe^{2+}$ and $Mn^{2+}$. The sample was allowed to react at 25, 30, and 35 °C for 150 min before being filtered. The concentrations of $F^-$, $Fe^{2+}$ and $Mn^{2+}$ in the filtrate were measured. Langmuir and Freundlich isotherm models were used to evaluate the maximum adsorption capacity and adsorption difficulty of Csrp for $F^-$, $Fe^{2+}$ and $Mn^{2+}$ (Matouq *et al.* 2015). The equations are as follows (Equations (5) and (6)):

Langmuir isotherm adsorption equation:

$$\frac{c_e}{q_e} = \frac{1}{(K_L q_m)} + \frac{c_e}{q_m} \tag{5}$$

Freundlich isotherm adsorption equation:

$$\ln q_e = \ln K_F + \frac{1}{n}\ln c_e \tag{6}$$

where $q_m$ is the adsorption capacity at adsorption saturation, mg/g; $K_L$ is the Langmuir constant, L/mg; and $K_F$ and $n$ are Freundlich empirical constants.

### Desorption and regeneration

To evaluate the availability of Csrp, Csrp with adsorbed ions was regenerated with 0.1 M $NaCO_3$ and 0.1 M $HNO_3$ solutions. Before this process, the adsorbed Csrp was pretreated, the unadsorbed ions on the surface of the Csrp were washed off with deionized water, filtered, and the Csrp was dried. The dried Csrp was added to 150 mL of $Na_2CO_3$ solution, and the mixture was shaken at 35 °C and 180 rpm for 150 min. Then, the Csrp was washed with deionized water to remove $Na_2CO_3$ from the surface. Subsequently, 150 mL of nitric acid solution was added to the Csrp, and the mixture was shaken at 35 °C and 180 rpm for 150 min. Next, the Csrp was washed with deionized water to remove nitric acid from the surface. Finally, the Csrp was dried at 110 °C for 2 h. After drying, the Csrp was regenerated, and the adsorption test was carried out again for completely desorbed Csrp for a total of five cycles.

## RESULTS AND DISCUSSION

### Optimization of the Srp modification methods

Natural Srp was modified by metal salt impregnation, acid–base activation and calcination, and the performance of the modified Srp in removing fluoride, iron and manganese was compared. The results are shown in Figure 1.

As shown in Figure 1(a), when the reaction time was less than 120 min, the removal rates of $F^-$, $Fe^{2+}$ and $Mn^{2+}$ by natural Srp all increased with increasing reaction time. As the reaction time continued to increase, the removal rates of $Fe^{2+}$ and $Mn^{2+}$ remained stable, while the removal rate of $F^-$ showed a downward trend. This is because with increasing reaction time, the increase in $OH^-$ released by Srp increases the electrostatic repulsion towards $F^-$, which affects the removal of $F^-$. In summary, 120 min was determined to be the best reaction time for natural Srp to adsorb $F^-$, $Fe^{2+}$, and $Mn^{2+}$. At this time, the removal rates of $F^-$, $Fe^{2+}$, and $Mn^{2+}$ were 73.4%, 92.1%, and 89.8%, respectively.

As shown in Figure 1(b), the removal rate of $F^-$ by metal salt-impregnated Srp increased with increasing metal salt concentration. This is because aluminium sulfate and calcium chloride adhere to the pores and surface of Srp, and when in contact with $F^-$ in solution, aluminium fluoride and calcium fluoride are generated and adsorbed on Srp, thus reducing the concentration of $F^-$ in solution (Zhai *et al.* 2010). The removal rates of $Fe^{2+}$ and $Mn^{2+}$ decreased with increasing metal salt concentration due to the enrichment of a large amount of $Al^{3+}$ and $Ca^{2+}$ in the modified Srp. These metal ions combine with the active groups in Srp to form complexes, occupying the effective sites for $Fe^{2+}$ and $Mn^{2+}$ adsorption on Srp. Additionally, due to a large amount of positively charged ions, the electrostatic repulsion towards $Fe^{2+}$ and $Mn^{2+}$ increases, which

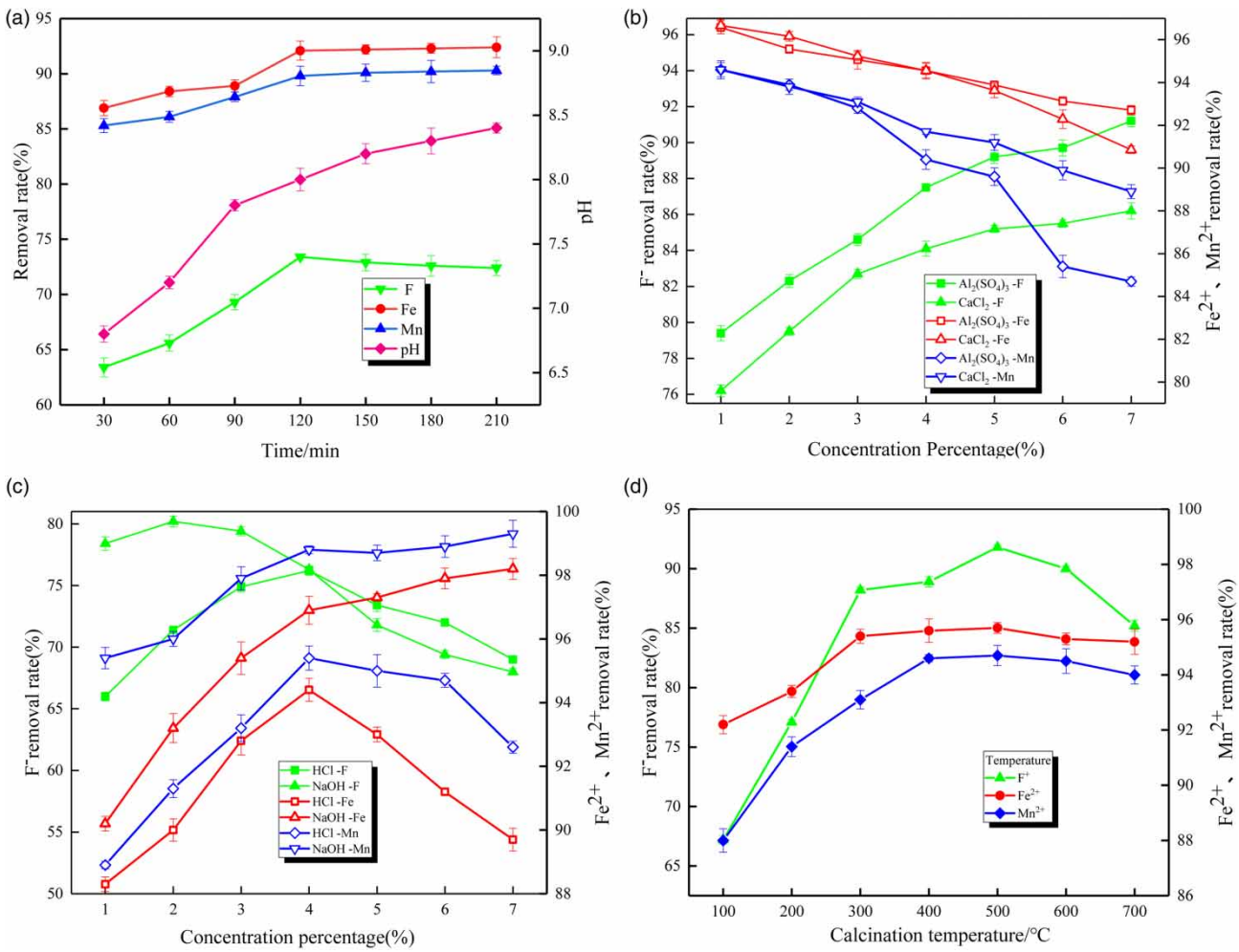


**Figure 1** | Removal rates of natural and modified Srp for fluoride, iron and manganese: (a) natural, (b) metal salt impregnation, (c) acid–base activation, and (d) calcination.

affects the removal of $Fe^{2+}$ and $Mn^{2+}$. In summary, fluoride, iron and manganese removal effects on the same concentration of metal-salt-impregnated Srp were opposite; thus, the simultaneous removal of all three ions could not be achieved.

Figure 1(c) shows that the removal rates of $F^-$, $Fe^{2+}$, and $Mn^{2+}$ are improved by modifying Srp with a proper amount of acid and base. This is because hydrochloric acid can dissolve impurities in Srp pores, thus improving its adsorption performance. Sodium hydroxide can chemically react with silica inside Srp to dissolve silicon, reduce the zeta potential, and improve the adsorption performance of Srp (Chen *et al.* 2021). When the concentration of hydrochloric acid exceeded 4%, the removal rates of $F^-$, $Fe^{2+}$, and $Mn^{2+}$ began to decrease, which may be due to the excessive acidity destroying the pores of the Srp and resulting in reduced adsorption performance (Gong *et al.* 2020). When the concentration of sodium hydroxide exceeded 2%, the $F^-$ removal rate showed a downward trend. This is because with increasing alkalinity, some surface particles are negatively charged and electrostatically repel $F^-$, which reduces the adsorption of $F^-$ on Srp. The removal rates of $Fe^{2+}$ and $Mn^{2+}$ increased with increasing sodium hydroxide concentration because $OH^-$ can form $Fe(OH)_2$ and $Mn(OH)_2$ precipitates with $Fe^{2+}$ and $Mn^{2+}$, thereby increasing the removal of $Fe^{2+}$ and $Mn^{2+}$. The acid–base activated Srp could not achieve the simultaneous removal of fluoride, iron and manganese.

As shown in Figure 1(d), when the calcination temperature did not exceed 500 °C, the removal rates of $F^-$, $Fe^{2+}$ and $Mn^{2+}$ gradually increased with increasing calcination temperature. This is because the surface water and interlayer water of Srp will be lost after calcination at a high temperature, which further enhances the hydrophilicity of the silicon oxygen structure in Srp and increases the contact performance between Srp and various ions. When the temperature exceeded 500 °C, the removal rates of $F^-$, $Fe^{2+}$ and $Mn^{2+}$ began to decrease because the high temperature may change the internal skeletal structure of Srp, resulting in changes in its crystal lattice, morphology and phase and a reduction in the removal of $F^-$, $Fe^{2+}$ and $Mn^{2+}$. Cao *et al.* (2017) used thermally activated Srp to adsorb cadmium and reached a similar conclusion. The adsorption capacity of thermally activated Srp was higher than that of natural Srp, and its adsorption capacity was strongly dependent on the activation temperature. After analysis and comparison, Srp calcined at 500 °C showed the best simultaneous removal of $F^-$, $Fe^{2+}$ and $Mn^{2+}$.

In conclusion, compared with natural Srp, the removals of $F^-$, $Fe^{2+}$ and $Mn^{2+}$ by Srp modified with metal salt impregnation, acid–base activation and calcination all improved. Overall, calcination at 500 °C showed the best effect among the various modifications, with $F^-$, $Fe^{2+}$ and $Mn^{2+}$ removal rates of 91.8%, 95.7% and 94.7%, respectively.

## Analysis of the factors influencing the removal of $F^-$, $Fe^{2+}$ and $Mn^{2+}$ on Csrp

### Influence of the adsorbent dose

The pH was kept at 6.5, the temperature was 25 °C, and the reaction time was 120 min. The effects of the Csrp dose on the removal rates of $F^-$, $Fe^{2+}$ and $Mn^{2+}$ were analysed, and the results are shown in Figure 2(a). When the dose of Csrp did not exceed 450 mg, the removal rates of $F^-$, $Fe^{2+}$, and $Mn^{2+}$ increased with an increasing dose of Csrp. This is because with an increasing Csrp dose, the relative specific surface area and adsorption sites of Csrp increase; thus, the removal rates of $F^-$, $Fe^{2+}$ and $Mn^{2+}$ gradually increase (Xie *et al.* 2020). When the dose of Csrp exceeded 450 mg, the removal rate of $F^-$ began to decrease, and the removal rates of $Fe^{2+}$ and $Mn^{2+}$ tended to be stable. This was because the $OH^-$ released into the water by the Csrp increased when the Csrp dose was increased. It can also be seen from the figure that the pH of the solution after the reaction increased as the Csrp dose increased. A large amount of $OH^-$ and $F^-$ resulted in electrostatic repulsion and a decrease in the $F^-$ removal rate. However, since the concentrations of $Fe^{2+}$ and $Mn^{2+}$ in the solution were constant, the removal rates of $Fe^{2+}$ and $Mn^{2+}$ remained basically unchanged as the Csrp dose continued to increase. In conclusion, when the Csrp dose was 450 mg (3 g/L), the removal effect of $F^-$, $Fe^{2+}$ and $Mn^{2+}$ was the best; the removal rates of $F^-$, $Fe^{2+}$ and $Mn^{2+}$ were 92.3%, 97.2% and 97.5%, respectively.

### Effect of the reaction time

The Csrp dose was kept at 450 mg, the pH was 6.5, and the temperature was 25 °C while the Csrp reaction time was changed to analyse its influence on the removal rates of $F^-$, $Fe^{2+}$ and $Mn^{2+}$. The results are shown in Figure 2(b). Over the period of 30–150 min, with increasing reaction time, the removal rates of $F^-$, $Fe^{2+}$ and $Mn^{2+}$ increased significantly. This is because during the initial stage of the reaction, the surface of the adsorbent contains a large number of adsorption sites, which fully combine with each ion in the test water sample and result in a large increase in the removal of each ion. When the reaction time exceeded 150 min, the removal rate of $F^-$ began to decrease, while the removal rates of $Fe^{2+}$ and $Mn^{2+}$ tended to be

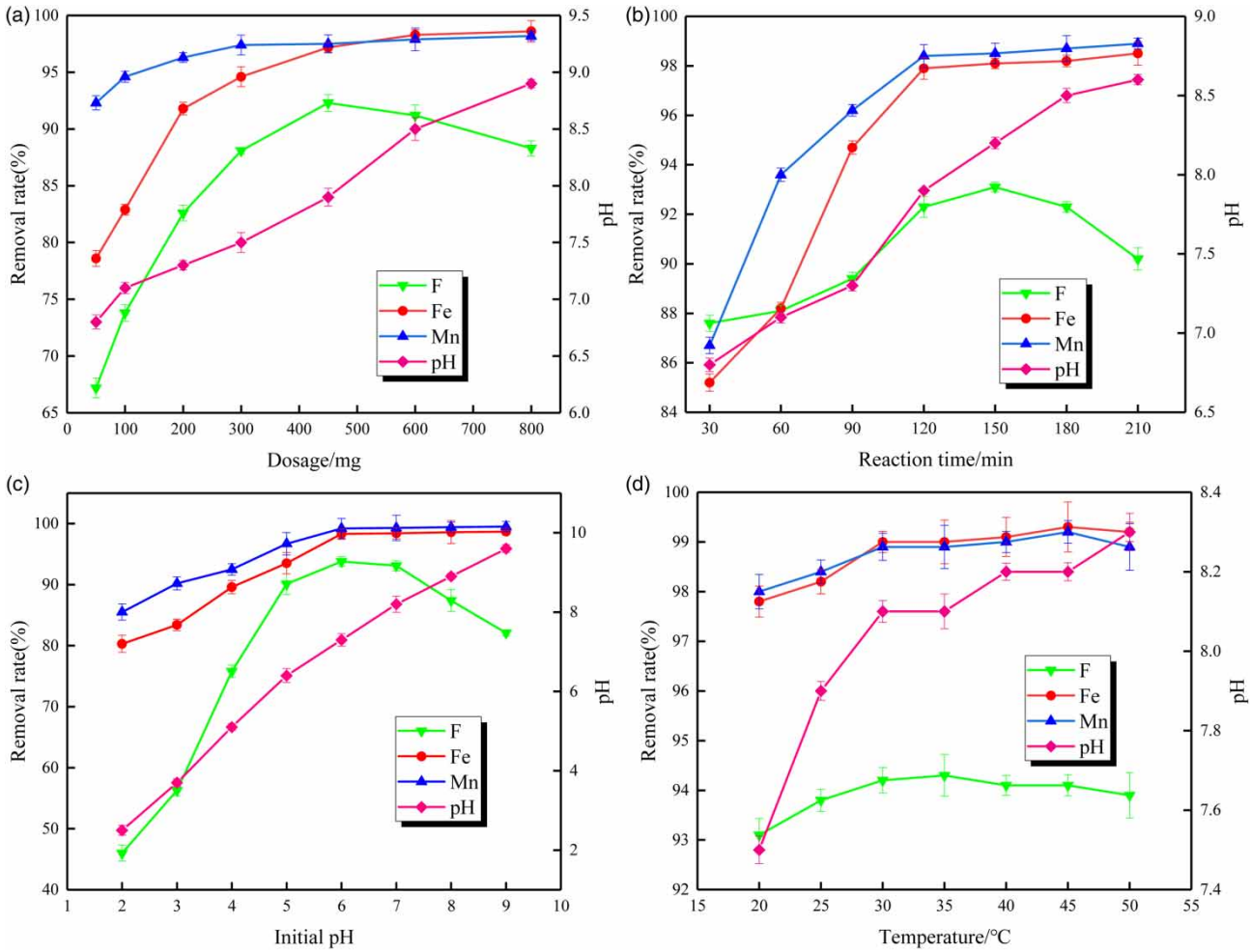


**Figure 2** | Removal rates of fluoride, iron and manganese by Csrp. Test conditions: (a) Csrp dose, (b) reaction time, (c) initial pH, and (d) reaction temperature.

stable. Considering the adsorption effects of $F^-$, $Fe^{2+}$ and $Mn^{2+}$, the optimal reaction time was determined to be 150 min, and the removal rates of $F^-$, $Fe^{2+}$ and $Mn^{2+}$ were 93.1%, 98.1% and 98.5%, respectively.

### Influence of the initial pH

The Csrp dose was maintained at 450 mg, the reaction time was 150 min, and the temperature was 25 °C while the initial pH of the water sample was changed to analyse its effect on the removal rates of $F^-$, $Fe^{2+}$ and $Mn^{2+}$ by Csrp, as shown in Figure 2(c). The removal efficiencies of $F^-$, $Fe^{2+}$ and $Mn^{2+}$ were poor when the pH was less than 4, probably due to the loss of the $Mg^{2+}$ active sites of the Csrp at lower pH (Sun *et al.* 2011). When the pH was 6, the $F^-$ removal rate reached its maximum because the Csrp surface was protonated and a positive charge was obtained. This increases the electrostatic attraction to $F^-$ and reduces the $F^-$ concentration. When the pH continued to increase, the $F^-$ removal rate began to decline because with increasing alkalinity, $OH^-$ in the solution began to compete with $F^-$ for adsorption, thereby decreasing the number of available adsorption sites. The removal rates of $Fe^{2+}$ and $Mn^{2+}$ increased with increasing pH. Due to the increase in pH, the content of $OH^-$ in solution increased, which promoted the removal of $Fe^{2+}$ and $Mn^{2+}$. After comprehensive consideration, the optimal reaction pH was determined to be 6, and the removal rates of $F^-$, $Fe^{2+}$ and $Mn^{2+}$ were 93.8%, 98.3% and 99.2%, respectively.

### Effect of the reaction temperature

The Csrp dose was kept at 450 mg, the reaction time was 150 min, and the pH was 6 while the reaction temperature was changed to analyse its influence on the removal rates of $F^-$, $Fe^{2+}$ and $Mn^{2+}$. The results are shown in Figure 2(d). When

the reaction temperature was between 20 and 35 °C, the removal rates of $F^-$, $Fe^{2+}$ and $Mn^{2+}$ increased with increasing temperature because the increase in temperature increased the activity of the reactants. From 35 to 45 °C, the removal rate of $F^-$ began to decrease, and the removal rates of $Fe^{2+}$ and $Mn^{2+}$ increased. This was caused by the increase in reaction temperature promoting the release of $OH^-$ from Csrp. When the temperature exceeded 45 °C, the removal rates of $F^-$, $Fe^{2+}$ and $Mn^{2+}$ all began to decrease. This may be due to the weakness of the adsorptive forces between the active site of the adsorbent and the adsorbate species and between the adjacent molecules of the adsorbed phase (Al-Anber & Al-Anber 2008). After comprehensive analysis, the optimal reaction temperature was determined to be 35 °C, and the removal rates of $F^-$, $Fe^{2+}$ and $Mn^{2+}$ were 94.3%, 99.0% and 98.9%, respectively.

Our research group previously studied a new type of adsorbent, Srp/HAP (Li *et al.* 2021b), whose $F^-$, $Fe^{2+}$, and $Mn^{2+}$ removal rates reached 98.6%, 99.9%, and 99.8%, respectively. Although the removal effect of Csrp is slightly lower than that of Srp/HAP, the preparation process of Csrp is simple, and the preparation cost is low. The most important thing is that the quality of the effluent treated by Csrp meets the drinking water standards set by the World Health Organization. Therefore, Csrp is also an excellent adsorbent for removing fluoride and iron and manganese.

### Analysis of removal of $F^-$, $Fe^{2+}$ and $Mn^{2+}$ by dealkalized Csrp

It can be seen from Figure 3 that the removal rates of $F^-$, $Fe^{2+}$ and $Mn^{2+}$ by dealkalized Csrp were lower than those by Csrp. This result may be due to the release of alkalinity by Csrp during the reaction, which caused some $Fe^{2+}$ and $Mn^{2+}$ to be removed by precipitation. The removal of $Fe^{2+}$ and $Mn^{2+}$ by dealkalized Csrp was due to adsorption. The removal rates of $Fe^{2+}$ and $Mn^{2+}$ reached 95.2% and 96.1% after 150 min, and these rates are only 3.8% and 2.8% lower than that of Csrp. It shows that the removal of $Fe^{2+}$ and $Mn^{2+}$ by Csrp mainly occurs via adsorption, and precipitation is only a small factor. The slight decrease in the $F^-$ removal rate may be due to the decrease in the $OH^-$ content in the dealkalized Csrp, which reduces the ion exchange between $F^-$ and $OH^-$.

### Kinetic analysis

The Csrp dose was kept at 450 mg, the pH was 6, and the reaction temperature was 35 °C. Samples were taken at pre-set times to determine the concentrations of $F^-$, $Fe^{2+}$ and $Mn^{2+}$ in the filtrate, and kinetic equation fitting was performed. The fitting curves are shown in Figure 4, and the fitting parameters are shown in Table 1.

It can be seen from the fitting curves in Figure 4 and the fitting results in Table 1 that the adsorption of $F^-$, $Fe^{2+}$ and $Mn^{2+}$ by Csrp is more in line with the quasi-second-order kinetic equation. The correlation coefficients ($R^2$) of the quasi-second-order kinetics for all ions are greater than 0.99, and the theoretical equilibrium adsorption capacities are closer to the

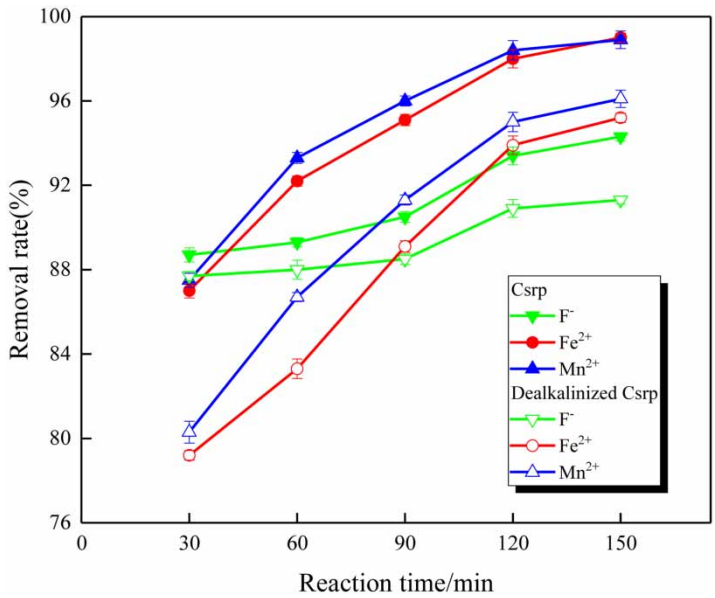


**Figure 3** | Comparison of the removal of $F^-$, $Fe^{2+}$ and $Mn^{2+}$ by dealkalized Csrp and the original Csrp.

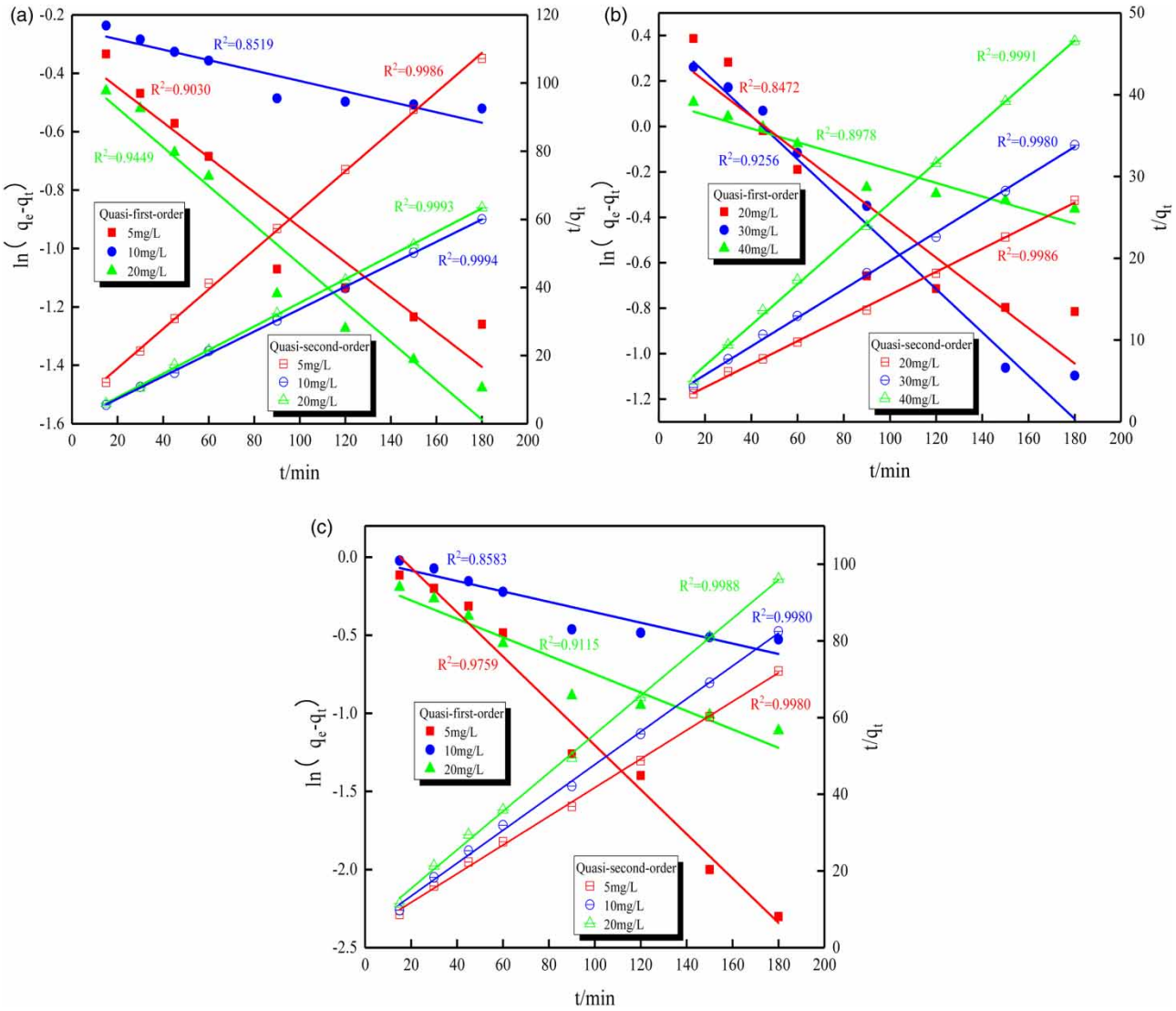


**Figure 4** | Kinetic equation fitting for (a) fluoride, (b) iron, and (c) manganese.

**Table 1** | Quasi-first-order and quasi-second-order kinetic fitting results

| | | Quasi-first-order dynamics | | | Quasi-second-order dynamics | | |
|---|---|---|---|---|---|---|---|
| **Ion type** | **Concentration mg/L** | $q_e$ mg/g | $k_1$/min$^{-1}$ | $R^2$ | $q_e$ mg/g | $k_2$/min$^{-1}$ | $R^2$ |
| $F^-$ | 5 | 0.7198 | 0.0138 | 0.9030 | 1.7198 | 0.0775 | 0.9986 |
| | 10 | 0.7807 | 0.0041 | 0.8519 | 3.0443 | 0.1184 | 0.9994 |
| | 20 | 0.6797 | 0.0154 | 0.9449 | 2.9202 | 0.1026 | 0.9993 |
| $Fe^{2+}$ | 20 | 1.4270 | 0.0179 | 0.8472 | 7.0827 | 0.0143 | 0.9986 |
| | 30 | 1.5342 | 0.0219 | 0.9256 | 5.7382 | 0.0135 | 0.9980 |
| | 40 | 1.1172 | 0.0069 | 0.8978 | 4.0246 | 0.0325 | 0.9991 |
| $Mn^{2+}$ | 5 | 1.2411 | 0.0327 | 0.9759 | 2.6714 | 0.0327 | 0.9980 |
| | 10 | 0.9807 | 0.0077 | 0.8583 | 2.3327 | 0.0377 | 0.9980 |
| | 20 | 0.8525 | 0.0136 | 0.9115 | 1.9884 | 0.0471 | 0.9988 |

experimental results. The quasi-second-order kinetic equation assumes that the adsorption rate is constrained by chemisorption (Wang *et al.* 2021), indicating that the removal of $F^-$, $Fe^{2+}$ and $Mn^{2+}$ by Csrp is mainly by chemisorption.

### Adsorption isotherm

The effects of different initial concentrations of $F^-$, $Fe^{2+}$ and $Mn^{2+}$ on the adsorption capacity of Csrp are shown in Figure 5 when the dose of Csrp was 450 mg, the pH was 6, and the reaction time was 150 min. Figure 5 shows that the adsorption capacities of $F^-$, $Fe^{2+}$ and $Mn^{2+}$ on Csrp increased with increasing reaction temperature and initial ion concentrations. With increasing initial ion concentrations, the active adsorption sites on the surface of the adsorbent gradually tend to be saturated, and thus, the adsorption capacity tends to plateau.

Table 2 shows the fitting results of the isothermal adsorption model. The correlation coefficient $R^2$ fitted by the Langmuir model for each ion is greater than 0.98, and the correlation coefficient $R^2$ fitted by the Freundlich model is greater than 0.96. The Langmuir isotherm model can better simulate the adsorption of $F^-$, $Fe^{2+}$ and $Mn^{2+}$ by Csrp, and the adsorption process of each ion conforms to monolayer adsorption. At 35 °C, the maximum monolayer saturated adsorption capacity $q_m$ values of Csrp for $F^-$, $Fe^{2+}$ and $Mn^{2+}$ were 6.6774 mg/g, 11.0473 mg/g and 9.9315 mg/g, respectively. Moreover, as seen from Table 3, Csrp has a higher adsorption capacity than most other adsorbents reported; thus, Csrp can be considered a potentially highly efficient adsorbent with the ability to synchronously remove $F^-$, $Fe^{2+}$ and $Mn^{2+}$ from aqueous solutions.

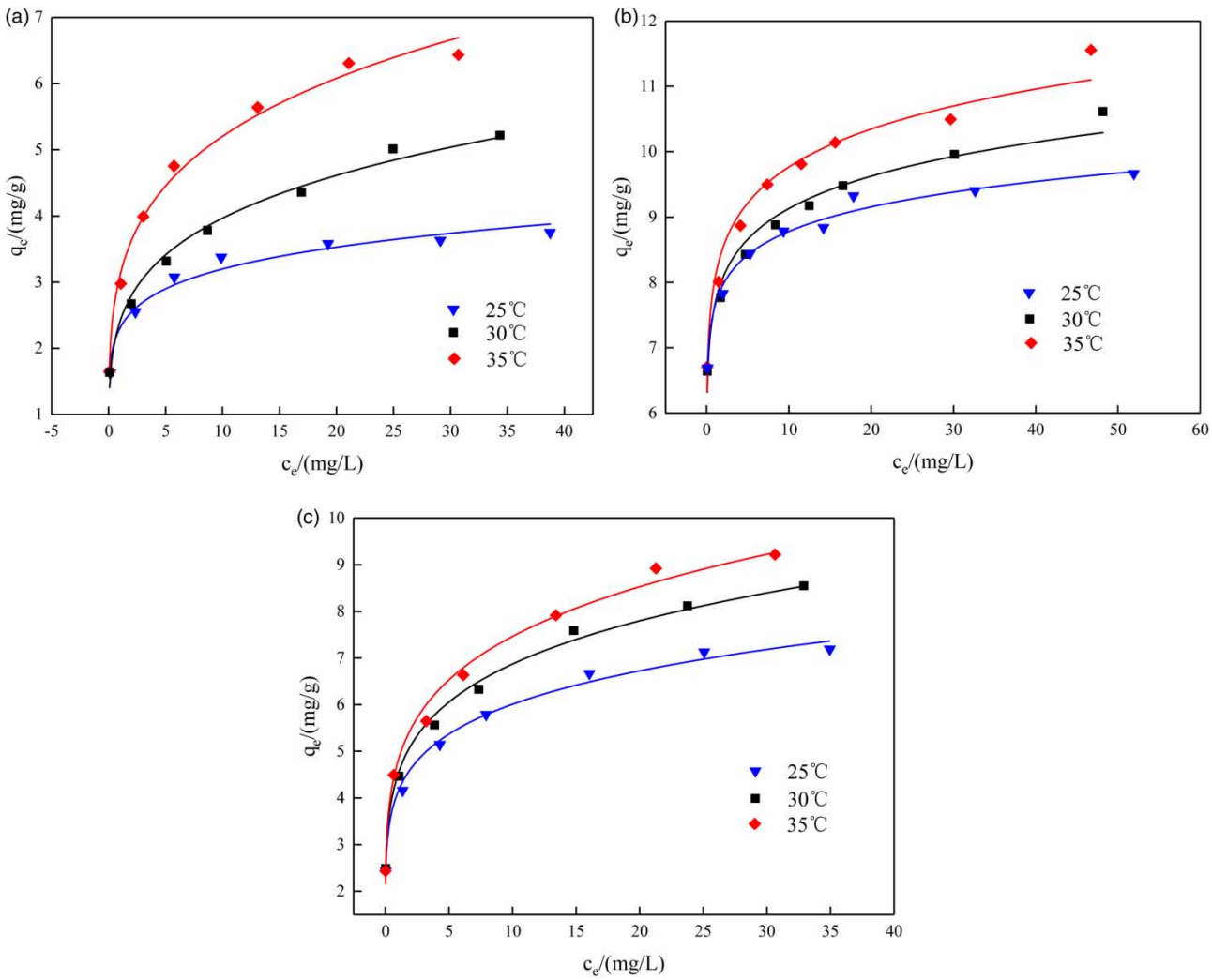


**Figure 5** | Isothermal adsorption curves of Csrp: (a) fluoride, (b) iron, and (c) manganese.

**Table 2** | Fitting parameters of the adsorption thermodynamics

| | | Langmuir | | | Freundlich | | |
|---|---|---|---|---|---|---|---|
| **Ion type** | **Temperature °C** | **$q_m$ (mg/g)** | **$K_L$** | **$R^2$** | **$K_F$** | **1/n** | **$R^2$** |
| $F^-$ | 25 | 3.8001 | 0.9994 | 0.9988 | 2.2539 | 0.1519 | 0.9793 |
| | 30 | 5.4212 | 0.4191 | 0.9859 | 2.5215 | 0.1958 | 0.9818 |
| | 35 | 6.6774 | 0.6539 | 0.9945 | 3.0642 | 0.2302 | 0.9947 |
| $Fe^{2+}$ | 25 | 9.4047 | 1.4628 | 0.9993 | 7.5058 | 0.0564 | 0.9858 |
| | 30 | 10.6530 | 0.8059 | 0.9969 | 7.7244 | 0.0721 | 0.9663 |
| | 35 | 11.0473 | 0.8264 | 0.9954 | 7.9446 | 0.0747 | 0.9635 |
| $Mn^{2+}$ | 25 | 7.7453 | 0.7759 | 0.9963 | 4.3481 | 0.1583 | 0.9920 |
| | 30 | 8.7352 | 0.6472 | 0.9927 | 4.6410 | 0.1685 | 0.9902 |
| | 35 | 9.9315 | 0.6741 | 0.9907 | 5.1335 | 0.1797 | 0.9911 |

**Table 3** | Comparison of the adsorption performance of different adsorbents for $F^-$, $Fe^{2+}$ and $Mn^{2+}$

| **Adsorbents** | **$q_e$ of $F^-$ (mg/g)** | **$q_e$ of $Fe^{2+}$ (mg/g)** | **$q_e$ of $Mn^{2+}$ (mg/g)** | **References** |
|---|---|---|---|---|
| Ti-zeolite | 1.511 | – | – | Ma *et al.* (2018) |
| Carboxylated chitosan beads | 1.385 | – | – | Viswanathan *et al.* (2009) |
| Natural stilbite zeolite modified with Fe(III) | 0.540 | – | – | Sun *et al.* (2011) |
| Granular activated carbon | – | 4.951 | 0.791 | Goher *et al.* (2015) |
| Amberlite IR-120H | – | 4.071 | 0.967 | |
| Slovakian natural zeolite | – | 1.157 | 0.075 | Shavandi *et al.* (2012) |
| Csrp | 1.572 | 6.600 | 1.648 | Present work |

## Analysis of adsorption regeneration

After five regeneration cycles, the removal rates of $F^-$, $Fe^{2+}$ and $Mn^{2+}$ by Csrp are shown in Figure 6. As shown in Figure 6, after five cycles of regeneration, the removal rates of $F^-$, $Fe^{2+}$ and $Mn^{2+}$ by Csrp decreased, which may be related to the incomplete elution of adsorbents. However, the removal rates of $F^-$, $Fe^{2+}$ and $Mn^{2+}$ remained above 83%, indicating that

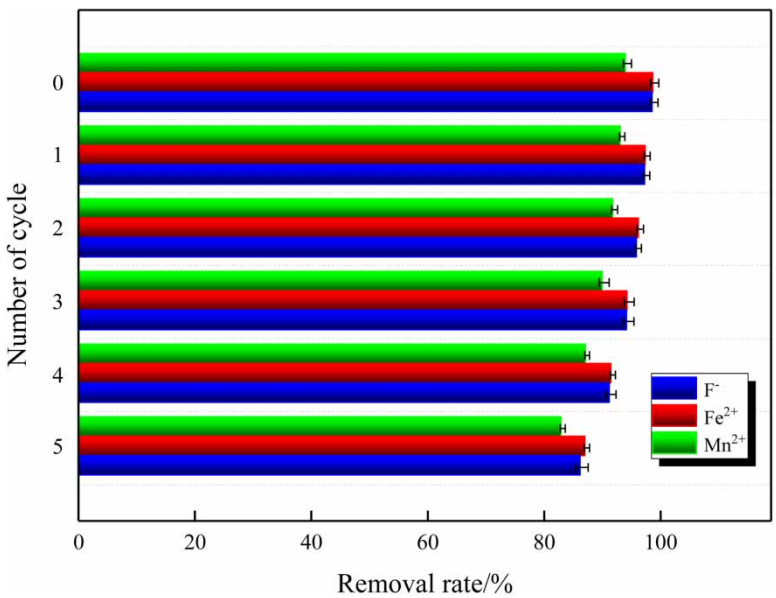


**Figure 6** | Percentages of $F^-$, $Fe^{2+}$ and $Mn^{2+}$ removal by Csrp in different cycles.

Csrp still had good reusability. Thus, Csrp can be used as an effective adsorption material for treating groundwater that contains $F^-$, $Fe^{2+}$ and $Mn^{2+}$.

### Evaluating the cost of the treatment

Both the effects of the treatment and the cost of the water treatment process should be considered. It can be seen from Table 4 that compared with membrane treatment and other adsorbents, Csrp water treatment has a lower cost, and its regeneration cost is reasonable.

## Microscopic characterization and adsorption mechanism analysis of Csrp

### X-ray diffraction analysis

Figure 7 shows the X-ray diffraction patterns of Srp and Csrp before and after adsorption. Figure 7 shows that Srp is mainly composed of $Mg_3Si_2(OH)_4O_5$ and that there are three characteristic peaks at $2\theta$ values of 12.16°, 24.68°, and 35.56°. The diffraction peaks of Csrp were consistent with natural Srp, indicating that the Srp structure was almost unchanged after calcination at 500 °C. After adsorption, new characteristic peaks appeared in Csrp, which were analysed by XRD software as $Fe_3Si_2(OH)_4O_5$, $Mn_3Si_2(OH)_4O_5$ and $MgSiF_6{\cdot}6H_2O$. It is speculated that $F^-$ can exchange ions with $OH^-$ and form organosilicon bonds with unsaturated Si-O-Si bonds. Additionally, an ion-exchange reaction of $Fe^{2+}$ and $Mn^{2+}$ with $Mg^{2+}$ occurred to form these three new substances (Li *et al.* 2003).

### SEM and EDS analysis

As shown in Figure 8(a), the surface of Srp presents a porous curled structure, and flaky structures are superimposed on each other on the surface. There are obvious textures and concave–convex structures among the textures. This special structure increases the specific surface area of Srp and gives Srp a certain physical adsorption capacity. As shown in Figure 8(b),

**Table 4** | Comparison of the cost of different water treatment materials

| Material cost | Water treatment cost (pound/m$^3$) | Regeneration cost (pound/kg) | References |
|---|---|---|---|
| $ESPA_2$4040 membrane (169.84 pound/piece) | 0.17 | – | Ma (2010) |
| Modified zeolite (0.04 pound/kg) | 0.10 | 0.022 | Zuo *et al.* (2019) |
| Csrp (0.03 pound/kg) | 0.09 | 0.017 | Present work |

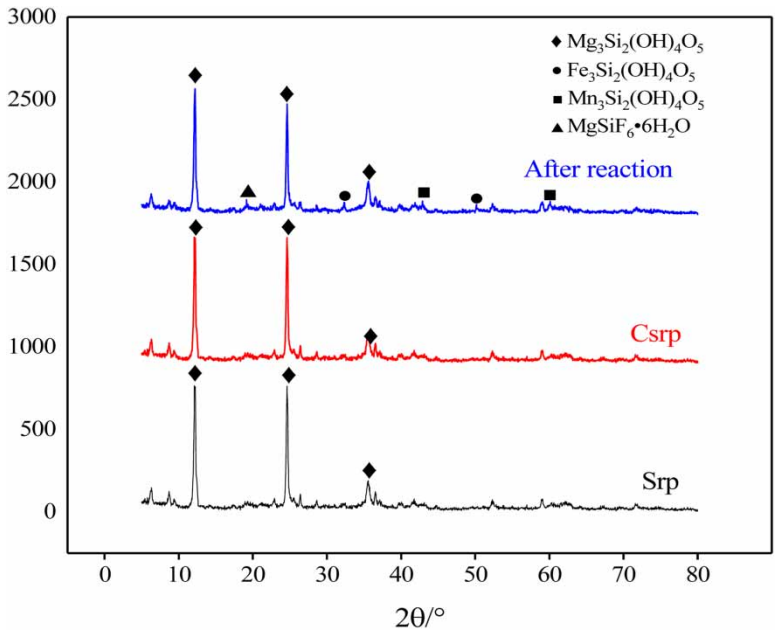


**Figure 7** | XRD patterns of Srp, Csrp and Csrp after reaction.

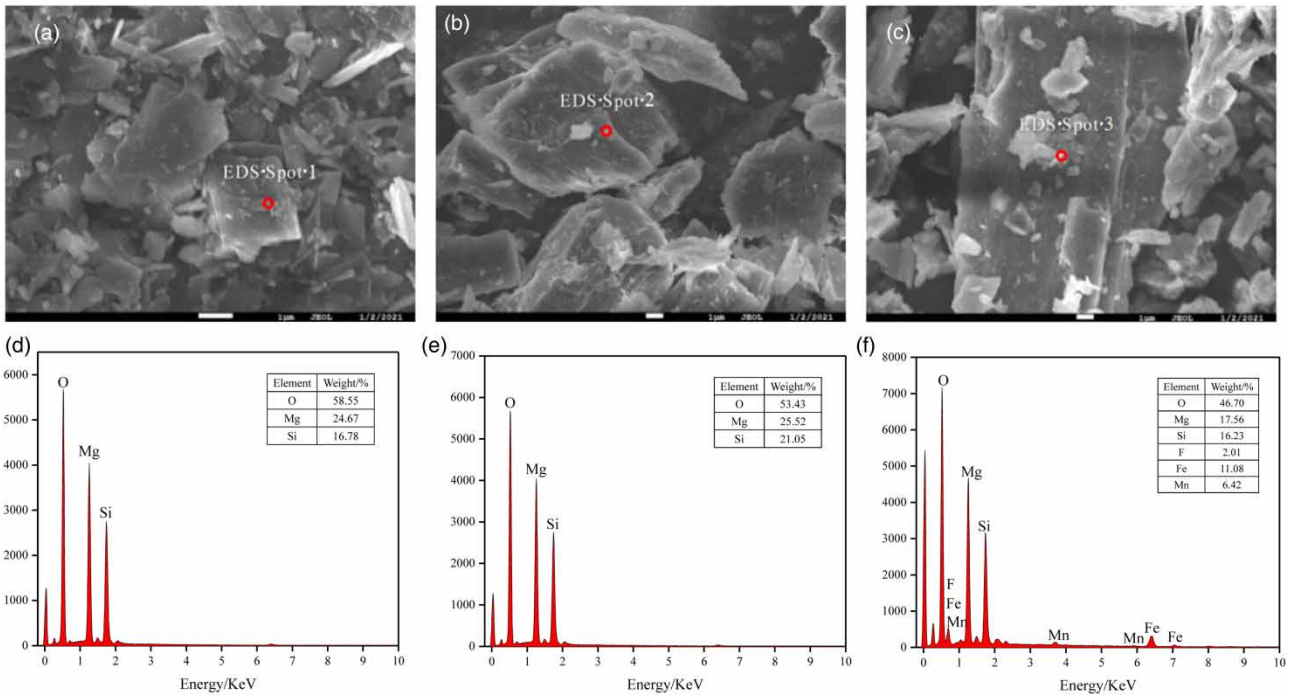


**Figure 8** | SEM images and EDS spectra of Srp and Csrp before and after reaction. SEM images of (a) Srp, (b) Csrp before reaction, and (c) Csrp after reaction. EDS images of (d) Srp, (e) Csrp before reaction, and (f) Csrp after reaction.

the surface structure of Srp calcined at 500 °C did not change significantly, indicating that the structure of Srp does not change significantly at a lower calcination temperature. Cao *et al.* (2019) used thermally activated Srp to adsorb $Pb^{2+}$ and found that the structure of Srp did not change significantly at a lower thermal activation temperature (<550 °C). The XRD analysis results of Srp before and after calcination were confirmed. As shown in Figure 8(c), after the treatment of the test water sample, the pores on the surface of Csrp became significantly smaller, and the amount of fine flocculent crystals increased. It is speculated that $F^-$, $Fe^{2+}$ and $Mn^{2+}$ may physically adsorb on the surface of Csrp or that a surface coordination reaction may have taken place.

Using an energy spectrometer to further determine the elements in the material, it can be seen from Figure 8(d) and 8(e) that Srp mainly contained O, Mg, and Si. After calcination, the content of O decreased, while the contents of magnesium and silicon increased, indicating that a dehydroxylation process occurred during the thermal activation of Srp. The EDS after adsorption (Figure 8(f)) showed F, Fe, and Mn, while the weight fraction of O decreased from 53.43% before adsorption to 46.70%, and the weight fraction of Mg decreased from 25.52% before adsorption to 17.53%. This further demonstrated that the ion-exchange reactions between $F^-$ and $OH^-$ and between $Fe^{2+}/Mn^{2+}$ and $Mg^{2+}$ are in good agreement with the XRD analysis results.

## FTIR spectroscopy

To understand the changes in the functional groups of Srp and Csrp before and after adsorption, FTIR spectroscopy was performed, and the results are shown in Figure 9. The infrared absorption peak of Csrp was very similar to that of natural Srp, indicating that the structure of serpentine did not change significantly after calcination and further confirming the XRD and SEM analysis results. The absorption peaks at 630.72 $cm^{-1}$ and 3,676.32 $cm^{-1}$ belonged to the Mg-OH stretching vibration. The absorption peaks of Csrp after adsorption were significantly weakened at these two points, indicating that ion-exchange reactions between $F^-$ and $OH^-$ and between $Fe^{2+}/Mn^{2+}$ and $Mg^{2+}$ occurred. In addition, the vibration peaks at 455.20 $cm^{-1}$ and 985.62 $cm^{-1}$ were attributed to Si-O bond stretching vibrations. After the reaction, the vibration peak of Csrp Si-O was weakened. This shows that $F^-$, $Fe^{2+}$, and $Mn^{2+}$ may undergo surface coordination with the unsaturated Si-O-Si bond. The absorption peak at 1,452.4 $cm^{-1}$ was $CO_3^{2-}$ (Selim *et al.* 2018), which may be because natural Srp absorbs $CO_2$ in the atmosphere and reacts to form carbonate groups. During the adsorption test, $CO_3^{2-}$ combined with $H^+$ in the solution to produce $CO_2$ gas that escaped; thus, the vibration peak of Srp at 1,452.4 $cm^{-1}$ disappeared after the reaction.

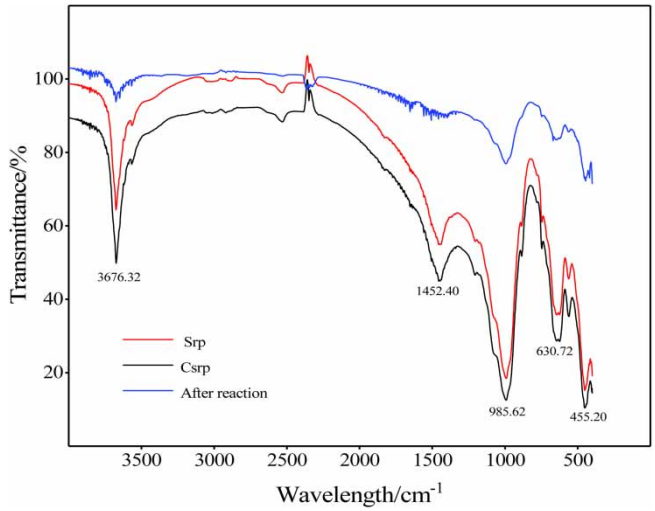


**Figure 9** | FTIR spectra of Srp and Csrp before and after reaction.

### Analysis of the removal mechanism

The removal of fluoride, iron and manganese by Csrp is mainly chemical adsorption, including ion exchange and surface coordination, and a small amount of metal ions is removed by precipitation. The specific analysis is as follows:

(1) Ion exchange: At the beginning of the reaction, there was more $H^+$ in the solution, which made the Csrp surface positively charged, and $F^-$ could be adsorbed to the Csrp surface by electrostatic attraction. As the reaction went on, the pH of the solution increased, resulting in more $OH^-$ in the solution, and $Fe^{2+}$ and $Mn^{2+}$ also accumulated on the Csrp surface due to electrostatic attraction. The Csrp then released an equivalent ion to exchange with it. The reaction equations are shown in (7) (8) and (9):

$$OH - Mg - OH + 2F^- \rightarrow F - Mg - F + 2OH^- \quad (7)$$

$$3Fe^{2+} + Mg_3Si_2(OH)_4O_5 \rightarrow Fe_3Si_2(OH)_4O_5 + 3Mg^{2+} \quad (8)$$

$$3Mn^{2+} + Mg_3Si_2(OH)_4O_5 \rightarrow Mn_3Si_2(OH)_4O_5 + 3Mg^{2+} \quad (9)$$

(2) Surface coordination: The unsaturated Si-O-Si bond has high chemical activity, can displace iron and manganese from the solution, and can adsorb fluoride to make it fixed on the surface. We found in FTIR analysis that the absorption peak of Si-O-Si was weakened, which further confirmed this speculation. The specific process is shown in Equations (10)–(12):

$$\equiv Si - O - Si \equiv + NaF \rightarrow \equiv Si - O - Na + \equiv Si - F \quad (10)$$

$$\equiv Si - O - Si \equiv + Fe - OH \rightarrow \equiv Si - O - Fe + \equiv Si - OH \quad (11)$$

$$\equiv Si - O - Si \equiv + Mn - OH \rightarrow \equiv Si - O - Mn + \equiv Si - OH \quad (12)$$

(3) Precipitation: Some iron and manganese may have been removed by precipitation because Csrp releases alkalinity during the reaction, resulting in an increase in the pH of the solution system, which in turn induces heavy metal ions to precipitate. Guo & Yuan (2000) also obtained similar conclusions in the serpentine adsorption test for heavy metal ions.

The specific removal process is shown in Figure 10.

## CONCLUSIONS

(1) Csrp has good performance in removing fluoride, iron and manganese. The best modification conditions were calcination at 500 °C for 120 min. The best conditions for Csrp to treat composite water samples with $F^-$, $Fe^{2+}$ and $Mn^{2+}$ at mass

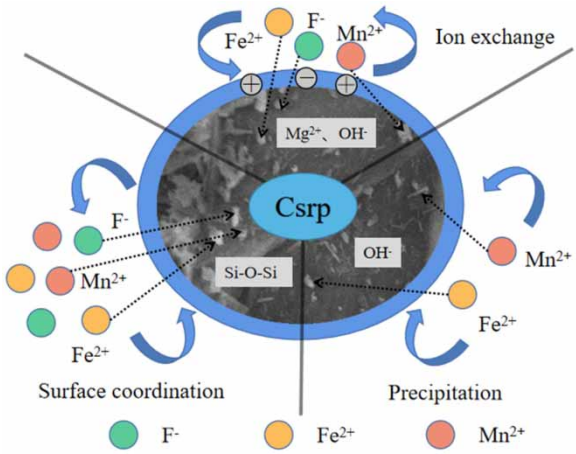


**Figure 10** | Schematic diagram showing the mechanism for removing fluoride, iron and manganese with Csrp.

concentrations of 5, 20 and 5 mg/L were as follows: a Csrp dose of 3 g/L, a pH of 6, a reaction temperature of 35 °C, and a reaction time of 150 min; the removal rates of $F^-$, $Fe^{2+}$ and $Mn^{2+}$ from the test water samples were 94.3%, 99.0%, and 98.9%, respectively. The quality of the treated water meets the drinking water standards set by the World Health Organization.

(2) The adsorption process of Csrp for the simultaneous removal of $F^-$, $Fe^{2+}$ and $Mn^{2+}$ was more in line with the quasi-second-order kinetic model and Langmuir model. This result indicated that Csrp not only physically adsorbed but also chemically adsorbed $F^-$, $Fe^{2+}$ and $Mn^{2+}$, and the adsorption process was single-layer adsorption.

(3) SEM, EDS, XRD, and FTIR spectroscopy were used to analyse Srp and Csrp before and after reaction. The results show that Srp underwent a dehydroxylation reaction during high-temperature calcination, which enhanced the ability of Srp to remove fluoride, iron and manganese. After reaction, new compounds, namely, $MgSiF_6{\cdot}6H_2O$, $Mn_3Si_2(OH)_4O_5$, and $Fe_3Si_2(OH)_4O_5$, were produced.

(4) After desorbing the adsorbed ions on Csrp, Csrp maintains good removal performance after five adsorption–desorption cycles. Csrp can be used as an excellent adsorbent for $F^-$, $Fe^{2+}$ and $Mn^{2+}$ in groundwater.

(5) At present, it is difficult to find adsorbents that can simultaneously remove fluoride, iron, and manganese. The adsorbents that we developed can achieve this effect. However, we are currently in the laboratory research stage, and other issues such as the amount of wastewater generated in the process of preparing future engineering applications need to be further studied.

## ACKNOWLEDGEMENTS

The authors acknowledge the support of National Key R&D Program of China (No. 2017YFC1503106), Scientific Research Project of Educational Department of Liaoning Province of China (LJKZ0344), Liaoning BaiQianWan Talents Program of China (No. 2018C01) and Liaoning Provincial Natural Science Foundation of China ((No. 2019-ZD-0037). Additionally, the authors thank AJE [www.aje.com] for English-language editing.

## DATA AVAILABILITY STATEMENT

All relevant data are included in the paper or its Supplementary Information.

## REFERENCES

Abri, A., Tajbakhsh, M. & Sadeghi, A. 2019 Adsorption of fluoride on a chitosan-based magnetic nanocomposite: equilibrium and kinetics studies. *Water Supply* **19** (1), 40–51.

Al-Anber, M. & Al-Anber, Z. A. 2008 Utilization of natural zeolite as ion-exchange and sorbent material in the removal of iron. *Desalination* **225** (1–3), 70–81.

Aziz, H. A., Tajarudin, H. A., Wei, T. H. L. & Alazaiza, M. Y. D. 2020 Iron and manganese removal from groundwater using limestone filter with iron-oxidized bacteria. *International Journal of Environmental Science and Technology* **17**, 2667–2680.

Barloková, D. & Ilavský, J. 2010 Removal of iron and manganese from water using filtration by natural materials. *Polish Journal of Environmental Studies* **19** (6), 1117–1122.

Cai, H., Chen, G., Peng, C., Xu, L., Zhang, Z., Ke, F. & Wan, X. 2015 Enhanced fluoride removal by loading Al/Zr onto carboxymethyl starch sodium: synergistic interactions between Al and Zr. *RSC Advances* **5** (123), 101819–101825.

Cao, C. Y., Liang, C. H., Yin, Y. & Du, L. Y. 2017 Thermal activation of serpentine for adsorption of cadmium. *Journal of Hazardous Materials* **329**, 222–229.

Cao, C. Y., Yu, B., Wang, M., Zhao, Y. Y. & Zhao, Y. H. 2019 Adsorption properties of $Pb^{2+}$ on thermal-activated serpentine. *Separation Science and Technology* **54** (18), 3037–3045.

Cattaneo, A., Gualtieri, A. F. & Artioli, G. 2003 Kinetic study of the dehydroxylation of chrysotile asbestos with temperature by in situ XRPD. *Physics and Chemistry of Minerals* **30** (3), 177–183.

Chaturvedi, S. & Dave, P. N. 2012 Removal of iron for safe drinking water. *Desalination* **303**, 1–11.

Chen, Y. L., Min, X. Y., Liu, Y., Xu, Z. F., Li, C. K. & Yu, J. H. 2021 Study on acid–base modification of waste brick and its removal performance of lead ions. *Technology of Water Treatment* **47** (5), 52–56.

Goher, M. E., Hassan, A. M., Abdel-Moniem, I. A., Fahmy, A. H., Abdo, M. H. & El-sayed, S. M. 2015 Removal of aluminum, iron and manganese ions from industrial wastes using granular activated carbon and Amberlite IR-120H. *The Egyptian Journal of Aquatic Research* **41** (2), 155–164.

Gong, Z. Y., Wang, C. Y., Zhao, F., Xu, D. Y., Luo, Q. Y. & Zhu, L. 2020 Effect of acid, alkali and salt modification on adsorption characteristics of oil vapour by activated carbon. *Chinese Journal of Environmental Engineering* **14** (5), 1276–1285.

Guo, J. X. & Yuan, C. G. 2000 Study on the adsorption of heavy metals in sewage by serpentine. *Fine Chemicals* **17** (10), 586–589.

Homoncik, S. C., MacDonald, A. M., Heal, K. V., Dochartaigh, B. É. Ó. & Ngwenya, B. T. 2010 Manganese concentrations in Scottish groundwater. *Science of the Total Environment* **408** (12), 2467–2473.

Huang, P., Li, Z., Chen, M., Hu, H., Lei, Z., Zhang, Q. & Yuan, W. 2017 Mechanochemical activation of serpentine for recovering Cu (II) from wastewater. *Applied Clay Science* **149**, 1–7.

Ijagbemi, C. O., Baek, M.-H. & Kim, D.-S. 2010 Adsorptive performance of un-calcined sodium exchanged and acid modified montmorillonite for $Ni^{2+}$ removal: equilibrium, kinetics, thermodynamics and regeneration studies. *Journal of Hazardous Materials* **174** (1–3), 746–755.

Jin, Z., Jia, Y., Zhang, K. S., Kong, L. T., Sun, B., Shen, W., Meng, F. L. & Liu, J. H. 2016 Effective removal of fluoride by porous MgO nanoplates and its adsorption mechanism. *Journal of Alloys and Compounds* **675**, 292–300.

Kwakye-Awuah, B., Sefa-Ntiri, B., Von-Kiti, E., Nkrumah, I. & Williams, C. 2019 Adsorptive removal of iron and manganese from groundwater samples in Ghana by zeolite Y synthesized from bauxite and kaolin. *Water* **11** (9), 1912.

Li, X. J., Wang, L. J., Lu, A. H. & Wang, C. Q. 2003 A discussion on activation mechanism of atom groups in serpentine. *Acta Petrologica et Mineralogica* **22** (4), 386–390.

Li, X. L., Yu, X. W., Li, L., Wang, L. G. & Liu, S. Y. 2021a Dynamic adsorption of fluorine, iron and manganese in groundwater of mining area by Srp/HAP. *Journal of China Coal Society* **46** (3), 1056–1066.

Li, X. L., Yu, X. W., Liu, L., Yang, J. L., Liu, S. Y. & Zhang, T. Y. 2021b Preparation, characterization serpentine-loaded hydroxyapatite and its simultaneous removal performance for fluoride, iron and manganese. *RSC Advances* **11** (27), 16201–16215.

Ma, Q. 2010 Comparison of application of Haideng 8040 membrane and 4040 membrane in reverse osmosis system. *Journal of Green Science and Technology* **10** (10), 174–175 + 179.

Ma, Z., Zhang, Q., Weng, X., Mang, C., Si, L., Guan, Z. & Cheng, L. 2018 Fluoride ion adsorption from wastewater using magnesium(II), aluminum(III) and titanium(IV) modified natural zeolite: kinetics, thermodynamics, and mechanistic aspects of adsorption. *Journal of Water Reuse and Desalination* **8** (4), 479–489.

Matouq, M., Jildeh, N., Qtaishat, M., Hindiyeh, M. & Al Syouf, M. Q. 2015 The adsorption kinetics and modeling for heavy metals removal from wastewater by *Moringa* pods. *Journal of Environmental Chemical Engineering* **3** (2), 775–784.

Meski, S., Tazibt, N., Khireddine, H., Ziani, S., Biba, W., Yala, S., , Sidane, D., Boudjouan, F. & Moussaoui, N. 2019 Synthesis of hydroxyapatite from mussel shells for effective adsorption of aqueous Cd(II). *Water Science and Technology* **80** (7), 1226–1237.

Mobarak, M., Mohamed, E. A., Selim, A. Q., Sellaoui, L., Lamine, A. B., Erto, A., Bonilla-Petriciolet, A. & Seliem, M. K. 2019 Surfactant-modified serpentine for fluoride and Cr(VI) adsorption in single and binary systems: experimental studies and theoretical modeling. *Chemical Engineering Journal* **369**, 333–343.

Patil, D. S., Chavan, S. M. & Oubagaranadin, J. U. K. 2016 A review of technologies for manganese removal from wastewaters. *Journal of Environmental Chemical Engineering* **4** (1), 468–487.

Selim, A. Q., Mohamed, E. A., Seliem, M. K. & Zayed, A. M. 2018 Synthesis of sole cancrinite phase from raw muscovite: characterization and optimization. *Journal of Alloys and Compounds* **762**, 653–667.

Shaban, M., Abukhadra, M. R., Khan, A. A. P. & Jibali, B. M. 2018 Removal of Congo red, methylene blue and Cr(VI) ions from water using natural serpentine. *Journal of the Taiwan Institute of Chemical Engineers* **82**, 102–116.

Shavandi, M. A., Haddadian, Z., Ismail, M. H. S., Abdullah, N. & Abidin, Z. Z. 2012 Removal of Fe(III), Mn(II) and Zn(II) from palm oil mill effluent (POME) by natural zeolite. *Journal of the Taiwan Institute of Chemical Engineers* **43** (5), 750–759.

Sun, Y., Fang, Q., Dong, J., Cheng, X. & Xu, J. 2011 Removal of fluoride from drinking water by natural stilbite zeolite modified with Fe(III). *Desalination* **277** (1–3), 121–127.

Viswanathan, N., Sundaram, C. S. & Meenakshi, S. 2009 Sorption behaviour of fluoride on carboxylated cross-linked chitosan beads. *Colloids and Surfaces B: Biointerfaces* **68** (1), 48–54.

Wang, W. B., Liu, D. F., Feng, D. M., Liu, Z. B. & Li, S. R. 2021 Study on preparation of cellulose hydrogel and its adsorption property for $Pb^{2+}$. *New Chemical Materials* **49** (5), 195–199.

Xie, X. M., Liao, M., Hua, J. Y., Chen, N., Zhang, N., Xu, P. Z., Xie, K. Z., Xu, C. X. & Liu, G. R. 2015 Adsorption–desorption characteristics of fermented rice husk for ferrous and sulfur ions. *Environmental Science* **36** (10), 3896–3905.

Xie, S., Xu, Y. M., Yan, C. X., Luo, W. W. & Sun, Y. B. 2020 Substructure characteristics of combined acid–base modified sepiolite and its adsorption for Cd(II). *Environmental Science* **41** (1), 293–303.

Yadav, K. K., Kumar, S., Pham, Q. B., Gupta, N., Rezania, S., Kamyab, H., Yadav, S., Vymazal, J., Kumar, V., Tri, D. Q., Talaiekhozani, A., Prasad, S., Reece, L. M., Singh, N., Maurya, P. K. & Cho, J. 2019 Fluoride contamination, health problems and remediation methods in Asian groundwater: a comprehensive review. *Ecotoxicology and Environmental Safety* **182**, 109362.

Zawar, M., Nazir, R., Hamid, A., Lima, E. C. & Shah, M. R. 2020 Rapid defluoridation of drinking water by calcium carbonate nanoadsorbent: characterization, adsorption studies and application to real samples' treatment. *Water Supply* **20** (2), 667–678.

Zhai, Y., Li, Z. W., Deng, Y. S., Wang, X. Y. & Tang, M. 2010 Experiment research on modified zeolite applied to adsorb fluorine ion from mine water. *Coal Science and Technology* **38** (9), 121–124.

Zhang, J. F., Luo, N. & Wang, X. C. 2009 Analysis of techniques for iron, manages removal and synchronous defluoridation of ground water. *China Rural Water and Hydropower* **2009** (5), 10–11 + 14.

Zuo, S. M., Jing, Z. Q., Tao, M. N., Tao, Z. K. & Wang, Y. 2019 Application of natural zeolite and modified zeolite in wastewater treatment. *Applied Chemical Industry* **48** (5), 1136–1139 + 1145.

First received 14 July 2021; accepted in revised form 4 December 2021. Available online 17 December 2021